# Adaptive Fractional-Order PID Control of PMSG based Wind Energy Conversion System for MPPT using Linear Observers

**Bo Yang [1], Tao Yu [2,*], Hongchun Shu [1], Yiming Han [1], Pulin Cao [1], and Lin Jiang [3]**

1 Faculty of Electric Power Engineering, Kunming University of Science and Technology, 650500 Kunming, China;
2 College of Electric Power, South China University of Technology, 510640 Guangzhou, China;
3 Department of Electrical Engineering & Electronics, University of Liverpool, Liverpool, L69 3GJ, United Kingdom;
* Correspondence: taoyu1@scut.edu.cn, Tel.: +86-130-020-88518

**Abstract:** This paper designs a novel adaptive fractional-order PID (AFOPID) control of a permanent magnetic synchronous generator (PMSG) based wind energy conversion system (WECS), which attempts to extract the maximum wind power by using a linear perturbation observer. The combinatorial effect of generator nonlinearities and parameter uncertainties, unmodelled dynamics, stochastic wind speed variation is aggregated into a perturbation, which is then estimated in the real-time by a linear extended-state observer (ESO) called high-gain state and perturbation observer (HGSPO). Besides, the perturbation estimate is employed as an auxiliary control signal which is fully compensated by a fractional-order PID (FOPID) controller to achieve a globally robust control consistency, simple structure and high reliability, as well as an improved tracking performance compared to that of PID control. In addition, AFOPID does not require an accurate PMSG model while only the measurement of d-axis current and mechanical rotation speed is required, which parameter is optimally tuned by particle swarm optimization (PSO). Four case studies are carried out, including step change of wind speed, low-turbulence stochastic wind speed, high-turbulence stochastic wind speed, and generator parameter uncertainties, respectively. Simulation results verify the effectiveness and superiority of AFOPID compared to that of PID, FOPID, and nonlinear control.

**Keywords:** PMSG; adaptive fractional-order PID control; WECS; high-gain state and perturbation observer

## Nomenclature

| *Variables* | | *Abbreviations* | |
|---|---|---|---|
| $v_{wind}$ | wind velocity | **MPPT** | maximum power point tracking |
| $\rho$ | air density | **PMSG** | permanent magnetic synchronous generator |
| $C_P$ | power coefficient | **VC** | vector control |
| $\lambda$ | tip-speed-ratio | **HGSPO** | high-gain state and perturbation observer |
| $\beta$ | blade pitch angle | **HGPO** | high-gain perturbation observer |
| $T_e$ | electromagnetic torque | **SPWM** | sinusoidal pulse-width modulation |
| $T_m$ | mechanical torque | **VSC** | voltage source converter |
| $\omega_e$ | electrical rotation speed | **PID** | proportional-integral-derivative |
| $\omega_m$ | mechanical rotation speed of turbine | **FLC** | feedback linearization control |
| $V_d, V_q$ | dq-axis stator voltages | **AFOPID** | adaptive fractional-order PID |
| $i_d, i_q$ | dq-axis currents | **WECS** | wind energy conversion system |
| ***System parameters*** | | ***AFOPID parameters*** | |
| $L_d, L_q$ | dq-axis inductances | $\alpha_j$ | Luenberger observer gains |
| $p$ | the number of pole pairs | $\epsilon_j$ | observer constant |
| $R$ | turbine radius | $B_0$ | constant control gain matrix |
| $J_{tot}$ | total inertia of the drive train | $K_{Pi}$ | proportional gain |
| $D$ | viscous damping coefficient | $K_{Ii}$ | integral gain |
| $R_s$ | stator resistance | $K_{Di}$ | derivative gain |
| $K_e$ | field flux | $\lambda_j$ | fractional differentiator order |
| $c_i$ | coefficients | $\mu_j$ | fractional integrator order |

## 1. Introduction

The continuously rising of energy demand and the urgent need to mitigate the malignant effects of climate changes resulted from global warming have driven an enormous variety of research interests to harness renewable energy sources in recent years [1-5]. Meanwhile, the severe issues associated with fast depleting reserves and ever-growing costs of fossil fuels such as oil, coal, and natural gas are also responsible for the growth and rise of emerging renewable energy applications, including hydro, wind, solar, and biomass, etc. [6].

Thus far, wind energy conversion system (WECS) plays a very crucial role and becomes very popular due to its elegant merits of cleanness, abundance, and wide distribution [7]. Variable speed wind turbine systems are normally based on either (a)

doubly-fed induction generator (DFIG) [8] or (b) permanent magnetic synchronous generator (PMSG) [9]. During the past decade, the deployment of PMSG has been considerably increased thanks to the prominent features of structure simplicity, energy production efficiency, gearless construction, self-excitation, and low noises [10].

One of the crucial tasks of PMSG is to extract the optimal power from varied wind speeds, also known as maximum power point tracking (MPPT) [11]. As a consequence, a proper controller design is quite crucial. At present, vector control (VC) associated with proportional-integral (PI) or proportional-integral-derivative (PID) loops has been widely adopted in both industrial application and academic research due to its structure simplicity and high reliability [12]. In general, such linear controllers are very useful to serve their purposes over a fixed set of operation points as they are mainly designed based on one-point linearized models of grid-connected PMSG systems. However, they are inadequate to achieve desired control performance under a wide variation of operation conditions, e.g., rapidly changing of wind speed.

Recently, fractional calculus based fractional-order PID (FOPID) control has been popularly investigated, which owns the potential to achieve improved control performance over the traditional PID controller because the differential order and integral order are introduced as adjustable controller parameters, thus its flexibility can be significantly increased [13]. In particular, reference [14] applied a fractional-order PI control for PMSG with different power converter topologies. In addition, a fuzzy FOPI+I controller was reported in [15] which offers effective control performance for MPPT and grid unity power factor. Besides, work [16] designed an FOPID controller based on analytical calculation and differential evolution algorithm for a permanent magnetic synchronous motor (PMSM) servo system. Nevertheless, the control performance of FOPID still degrades under varied operation conditions due to the inherent flaws of linear control framework.

Alternatively, various nonlinear robust/adaptive control schemes have provided another perspective to address such challenges by carefully examining the PMSG dynamics or the typical characteristics of wind. In literature [17], a feedback linearization control (FLC) was proposed to globally remove all the nonlinearities of PMSG for MPPT, which however requires an accurate system model and lack of robustness against any modelling uncertainties. In order to enhance the robustness of PMSG, a nonlinear backstepping control was devised to tackle stochastic wind speed variations which stability is assured by Lyapunov analysis [18]. In work [19], a model predictive control (MPC) and dead-beat predictive control strategies were developed to forecast the possible future behaviour of the control variables of PMSG. Furthermore, a nonlinear Luenberger-like observer was used to estimate the mechanical variables by only the measurement of electrical variables of PMSG to achieve MPPT [20]. Additionally, an enhanced exponential reaching law based sliding-mode control (SMC) was presented for PMSG to reduce the malignant chattering issues and to improve total harmonics distortion property [21]. Meanwhile, an improved sliding mode model reference adaptive system (SM-MRAS) speed observer based fuzzy controller was designed for MPPT, which implementation feasibility is validated by a small-capacity PMSG while the converter is controlled by digital signal processing (DSP) platform [22]. In general, these advanced control strategies can usually provide a quite satisfactory control performance but may also result in a quite complicated structure, which often limits their implementation in practice.

The aforementioned discussions have revealed such an annoying dilemma: Nonlinear robust/adaptive control can offer the merits of globally robust control consistency with the demerits of complicated control structure, while FOPID control can provide the advantages of significant simplicity and high reliability with the disadvantages of control inconsistency. Such a tricky contradiction motivates the authors to develop a novel hybrid control framework, which attempts to appropriately exploit their prominent strength along with an aim to reduce their notorious weakness, such that a proper trade-off could be realized. Hence, an adaptive FOPID (AFOPID) is proposed with the use of linear extended-state observer (ESO) called high-gain state and perturbation observer (HGSPO) [23,24]. The contribution and novelty of this paper can be summarized as the following four aspects:

- The combinatorial effect of generator nonlinearities and parameter uncertainties, unmodelled dynamics, wind speed randomness, is aggregated into a perturbation, which is estimated by an HGSPO in real-time. Hence, AFOPID is able to effectively tackle different types of uncertainties and can be applied for plenty of practical problems;
- FOPID framework is employed which outperforms conventional PID control in terms of reduced overshoot and settling time, thus it can considerably improve the control performance, together with a simple structure and high reliability;
- AFOPID does not require an accurate PMSG model while only the d-axis current and mechanical rotation speed need to be measured, which control parameters are optimally tuned by particle swarm optimization (PSO). Moreover, a fully decoupled control of d-axis current and mechanical rotation speed could be realized;
- The advantage of globally robust control consistency of nonlinear robust/adaptive control and superiority of structure simplicity of linear control are beneficially incorporated by the proposed approach.

The rest of the paper is organized as follows: Section 2 is devoted to develop the PMSG model. In Section 3, AFOPID is presented while Section 4 designs the AFOPID of PMSG for MPPT. Case studies are carried out in Section 5. Lastly, conclusions are summarized in Section 6.

## 2. Modelling of PMSG based Wind Energy Conversion System

Figure 1 illustrates the configuration of a PMSG system which is connected to the power grid bus via back-to-back voltage source converter (VSC). The produced active power and reactive power of PMSG is regulated through the generator-side VSC, while the grid-side VSC attempts to deliver active power to the power grid through the DC-link and to maintain the DC-link voltage at the rated value. Two VSCs are controlled independently while the dynamics of the PMSG and the power grid is fully decoupled via the DC-link [17,25]. As the MPPT mainly relies on the control of the generator-side VSC, the dynamics of grid-side VSC is ignored in this paper.

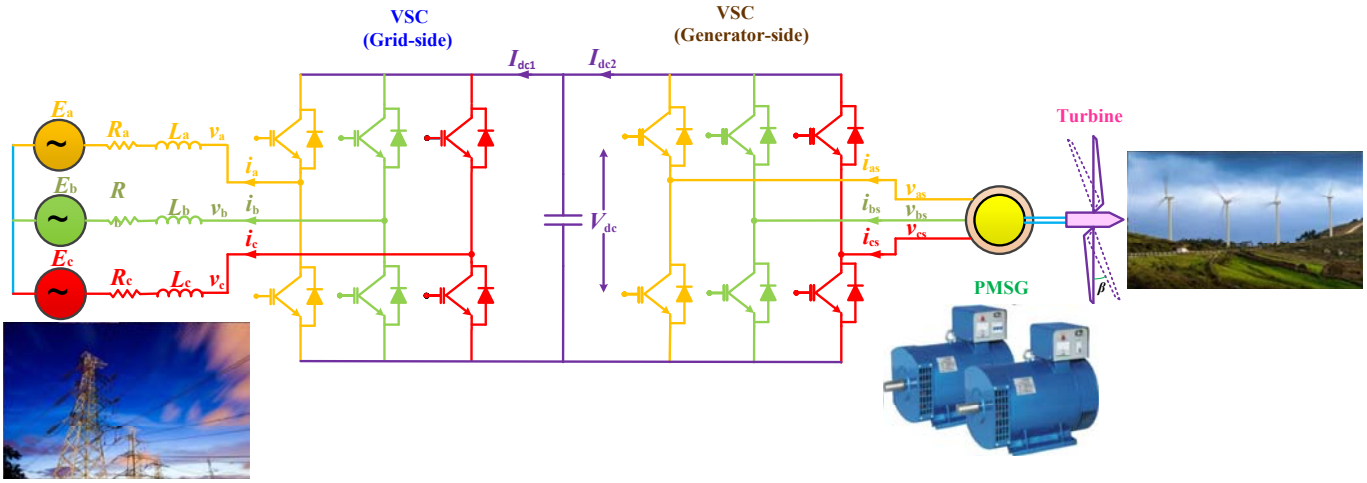


**Figure 1.** The configuration of a PMSG based WECS.

### *2.1 Variable speed wind turbine modelling*

The tip-speed-ratio $\lambda$ of wind turbine is defined as

$$\lambda = \frac{\omega_{\mathrm{m}} R}{v_{\mathrm{wind}}} \tag{1}$$

where $\omega_{\mathrm{m}}$ denotes the mechanical rotation speed of wind turbine and $v_{\mathrm{wind}}$ represents the wind speed; $R$ is the blade radius of wind turbine, respectively. According to the wind turbine dynamics, the power coefficient $C_{\mathrm{p}}(\lambda,\beta)$ can be described by [17,25]

$$C_{\mathrm{p}}(\lambda,\beta) = c_1\left(\frac{c_2}{\lambda_i} - c_3\beta - c_4\right)e^{-\frac{c_5}{\lambda_i}} \tag{2}$$

with

$$\frac{1}{\lambda_i} = \frac{1}{\lambda+0.08\beta} - \frac{0.035}{\beta^3+1} \tag{3}$$

where the coefficients $c_1$ to $c_5$ are selected as $c_1$=0.22, $c_2$=116, $c_3$=0.4, $c_4$=5, and $c_5$=12.5, respectively [17,25]. In addition, $\beta$ denotes the pitch angle;

Furthermore, the mechanical power extracted by the wind turbine from various wind speeds is determined by

$$P_{\mathrm{m}} = \frac{1}{2}\rho\pi R^2 C_{\mathrm{p}}(\lambda,\beta) v_{\mathrm{wind}}^3 \tag{4}$$

where $\rho$ represents the air density. During MPPT the wind turbine only operates in the sub-rated speed range, thus its pitch control is deactivated.

### *2.2 Permanent magnetic synchronous generator modelling*

The dynamics of PMSG in the d-q reference frames are written as [17,25]

$$V_d = i_d R_s + L_d\frac{di_d}{dt} - \omega_e L_q i_q \tag{5}$$

$$V_q = i_q R_s + L_q\frac{di_q}{dt} + \omega_e(L_d i_d + K_e) \tag{6}$$

$$T_e = p[(L_d - L_q)i_d i_q + i_q K_e] \tag{7}$$

where $V_{\mathrm{d}}$ and $V_{\mathrm{q}}$ are the stator voltages in the d-q axis; $R_{\mathrm{s}}$ is the stator resistance; $L_{\mathrm{d}}$ and $L_{\mathrm{q}}$ are d-q axis inductances; $i_{\mathrm{d}}$ and $i_{\mathrm{q}}$ are the currents in the d-q axis; $\omega_e = p\omega_m$ is the electrical rotation speed; $K_{\mathrm{e}}$ is the permanent magnetic flux given by the magnets; and $p$ is the number of pole pairs, respectively.

### *2.3 Mechanical shaft system modelling*

The dynamics of mechanical shaft system and mechanical torque of PMSG are given by [17,25]

$$J_{\mathrm{tot}}\frac{\mathrm{d}\omega_{\mathrm{m}}}{\mathrm{d}t} = T_{\mathrm{m}} - T_{\mathrm{e}} - D\omega_{\mathrm{m}} \tag{8}$$

$$T_{\mathrm{m}} = \frac{1}{2}\rho\pi R^5\frac{C_{\mathrm{p}}(\lambda,\beta)}{\lambda^3}\omega_{\mathrm{m}}^2 \tag{9}$$

where $J_{\mathrm{tot}}$ is the total inertia of the drive train which equals to the summation of wind turbine inertia constant and generator inertia constant; $D$ is the viscous damping coefficient; $T_{\mathrm{m}}$ is the mechanical torque of the wind turbine, respectively. In addition, active power is calculated as

$$P_{\mathrm{e}} = T_{\mathrm{e}}\omega_{\mathrm{m}} \tag{10}$$

with $T_{\mathrm{e}}$ being the electromagnetic torque.

In order to achieve MPPT, the power coefficient $C_{\mathrm{p}}(\lambda,\beta)$ should be maintained at its maximum point $C_{\mathrm{p}}^{*}$ at various wind speeds within the operation range. The pitch angle is taken as $\beta = 2°$, the optimal tip-speed-ratio $\lambda^{*} = 7.4$ while maximum power coefficient $C_{\mathrm{p}}^{*} = 0.4019$ [17,25].

## 3. Adaptive Fractional-Order PID Control Design

### *3.1 Linear observer based perturbation estimation*

Consider an uncertain nonlinear system with the following canonical form

$$\begin{cases} \dot{x} = Ax + B(a(x) + b(x)u + d(t)) \\ y = x_1 \end{cases} \tag{11}$$

where $x = [x_1, x_2, \cdots, x_n]^{\mathrm{T}} \in R^n$ is the state variable vector; $u \in R$ and $y \in R$ are the control input and system output, respectively; $a(x)$: $R^n \mapsto R$ and $b(x)$: $R^n \mapsto R$ are unknown smooth functions which represent the aggregated effect of nonlinearities, parameter uncertainties, and unmodelled dynamics; and $d(t)$: $R^+ \mapsto R$ represents the time-varying external disturbances. The state matrix $A$ and state matrix $B$ are of the canonical form as follows:

$$A = \begin{bmatrix} 0 & 1 & 0 & \cdots & 0 \\ 0 & 0 & 1 & \cdots & 0 \\ \cdots & \cdots & \cdots & \cdots & \cdots \\ 0 & 0 & 0 & \cdots & 1 \\ 0 & 0 & 0 & \cdots & 0 \end{bmatrix}_{n\times n}, B = \begin{bmatrix} 0 \\ 0 \\ \vdots \\ 0 \\ 1 \end{bmatrix}_{n\times 1} \tag{12}$$

The perturbation of system (11) is defined as [23,24,26]

$$\psi(x,u,t) = a(x) + (b(x) - b_0)u + d(t) \tag{13}$$

where $b_0$ is a user-defined constant control gain, by which the uncertainties of the control gain $b(x)$ can be aggregated into the perturbation.

From the original system (11), the last state, e.g., $x_n$, is rewritten as follows

$$\dot{x}_n = a(x) + (b(x) - b_0)u + d(t) + b_0 u = \psi(x,u,t) + b_0 u \tag{14}$$

Here, state (14) is consisted of two terms, e.g., perturbation term $\psi(x,u,t)$ which contains all types of uncertainties and control term $b_0 u$ which is user-determined.

Define an extended state to describe the perturbation term, e.g., $x_{n+1} = \psi(x,u,t)$. Then, system (11) can be directly extended into

$$\begin{cases} y = x_1 \\ \dot{x}_1 = x_2 \\ \vdots \\ \dot{x}_n = x_{n+1} + b_0 u \\ \dot{x}_{n+1} = \dot{\psi}(\cdot) \end{cases} \tag{15}$$

Therefore, the extended state $x_{n+1}$ is able to separate the unknown perturbation term from the original state $x_n$.

The extended state vector is written as $x_{\mathrm{e}} = [x_1, x_2, \cdots, x_n, x_{n+1}]^{\mathrm{T}}$ for the purpose of simple representation of Eq. (15), with the following two assumptions [23,24,26]

**A.1** $b_0$ is chosen to satisfy: $|\boldsymbol{b(x)/b_0 - 1}| \le \boldsymbol{\theta < 1}$, where $\theta$ is a positive constant.

**A.2** The function $\boldsymbol{\psi(x,u,t)}$: $\boldsymbol{R^n \times R \times R^+ \mapsto R}$ and $\boldsymbol{\dot{\psi}(x,u,t)}$: $\boldsymbol{R^n \times R \times R^+ \mapsto R}$ are locally Lipschitz in their arguments and bounded over the domain of interest, with $\boldsymbol{\psi}$(0,0,0)=0 and $\boldsymbol{\dot{\psi}}$(0,0,0)=0.

Here, Assumption **A.2** is used to guarantee that the closed-loop system is ultimately bounded under HGSPO and the proposed control law. Moreover, Assumption **A.1** is used, together with consideration of the perturbation assumed as a smooth function of time, to ensure the existence of the bounds of perturbation and its derivative as described by assumption **A.2**. The detailed proof can be found in reference [26] for interested readers.

Throughout this paper, $\boldsymbol{\tilde{x} = x - \hat{x}}$ refers to the estimation error of $x$ whereas $\boldsymbol{\hat{x}}$ represents the estimate of $x$, together with $x^*$ denotes the reference of variable $x$. Design an ($n$+1)th-order HGSPO for the extended system (15) to simultaneously estimate the states and perturbation, it gives [23,24,26]

$$\dot{\hat{x}}_{\mathrm{e}} = A_0 \hat{x}_{\mathrm{e}} + B_1 u + H(x_1 - \hat{x}_1) \tag{16}$$

with

$$A_0 = \begin{bmatrix} 0 & 1 & 0 & \cdots & 0 \\ 0 & 0 & 1 & \cdots & 0 \\ \cdots & \cdots & \cdots & \cdots & \cdots \\ 0 & 0 & 0 & \cdots & 1 \\ 0 & 0 & 0 & \cdots & 0 \end{bmatrix}_{(n+1)\times(n+1)} , B_1 = \begin{bmatrix} 0 \\ 0 \\ \vdots \\ 1 \\ 0 \end{bmatrix}_{(n+1)\times 1} \tag{17}$$

where $A_0$ and $B_1$ are the extended state matrix and extended control matrix, respectively; observer gain $H = [\alpha_1/\varepsilon, \alpha_2/\varepsilon^2, \ldots, \alpha_n/\varepsilon^n, \alpha_{n+1}/\varepsilon^{n+1}]^{\mathrm{T}}$ which determines the estimation rate; thickness layer boundary of observer $0 \le \varepsilon \ll 1$, such that a high-gain could be achieved; and Luenberger observer gains $\alpha_i$, $i$ = 1, 2,⋯, $n$ + 1, are chosen to place the poles of polynomial $s^{n+1} + \alpha_1 s^n + \alpha_2 s^{n-1} + \cdots + \alpha_{n+1} = (s + \lambda_\alpha)^{n+1} = 0$ being in the open left-half complex plane at $-\lambda_\alpha$, with

$$\alpha_i = C_{n+1}^i \lambda_\alpha^i, i = 1,2,\cdots,n+1. \tag{18}$$

where $\lambda_\alpha$ denotes the observer root which guarantees the convergence of observer. In addition, $C_{n+1}^i = \frac{(n+1)!}{i!*(n+1-i)!}$.

### *3.2 Fractional-order PID control framework*

Fractional calculus (FC) is an extension of regular integral calculus (IC) to non-integer case. In comparison to IC, FC is adequate and natural to fully characterize many physical phenomena. In general, the extra degrees of freedom from the use of fractional-order integrator and differentiator could further enhance the control performance compared with that of traditional integer-order controller. The non-integer order fundamental operator ${}_a\mathrm{D}_t^\alpha$ is defined as [28,29] where $a$ and $t$ are the lower and upper limits and $\alpha \in R$ is the operation order. Here, Riemann-Liouville (RL) definition for fractional-order derivative is used.

FOPID control attracts an increasing amount of interest from the control domain, which is based on the use of a fractional integrator of order $\mu$ and a fractional differentiator of order $\lambda$, instead of the classical integer order integrator and differentiator. Previous studies [14-16] have proved that such generalization can realize an improved shaping of the closed-loop system dynamical responses thanks to the introduction of the two supplementary tuning parameters.

The transfer function $G(s)$ of FOPID control is given by

$$G(s) = K_P + \frac{K_I}{s^\mu} + K_D s^\lambda \tag{19}$$

where $K_P$, $K_I$ and $K_D$ are the proportional gain, integral gain, and derivative gain, respectively. Moreover, $\mu$ and $\lambda$ (between 0 to 2) denote the fractional integrator order and fractional differentiator order, respectively.

### *3.3 Adaptive fractional-order PID control*

The AFOPID control for system (11) can be designed as

$$u = \frac{1}{b_0}[x_1^{*(n)} - \hat{\psi}(\cdot) + K_\mathrm{P}(x_1 - x_1^*) + \frac{K_\mathrm{I}}{s^\mu}(x_1 - x_1^*) + K_\mathrm{D} s^\lambda (x_1 - x_1^*)] \tag{20}$$

where $x_1^*$ denotes the reference of state $x_1$ while $x_1^{*(n)}$ is the $n$th-order derivative of reference $x_1^*$.

Figure 2 illustrates the overall control framework of AFOPID with PSO for the control parameter tuning. From Fig. 2, one can find that perturbation estimate compensation, e.g. $-\hat{\psi}(\cdot)$, is introduced to achieve an adaptive control performance as it can fully compensate the effect of various uncertainties. The adaptive control performance through such perturbation estimation and compensation has been proved in reference [24]. On the other hand, FOPID framework, e.g., $K_\mathrm{P}(x_1 - x_1^*) + \frac{K_\mathrm{I}}{s^\mu}(x_1 - x_1^*) + K_\mathrm{D} s^\lambda (x_1 - x_1^*)$, is synthesized to realize an improved tracking performance compared to that of PID control thanks to the use of fractional integrator and a fractional differentiator, which has been proved in reference [28]. Lastly, particle swarm optimization (PSO) [35] is employed to optimally tune the control parameters of AFOPID. As a result, AFOPID control is developed via a proper hybrid of the nonlinear perturbation estimation based approach and the linear FOPID framework, which can beneficially exploits the merits of linear control and nonlinear control, with moderate control structure complexity in comparison to linear control (low control structure complexity) [27] and nonlinear control (high control structure complexity) [24].

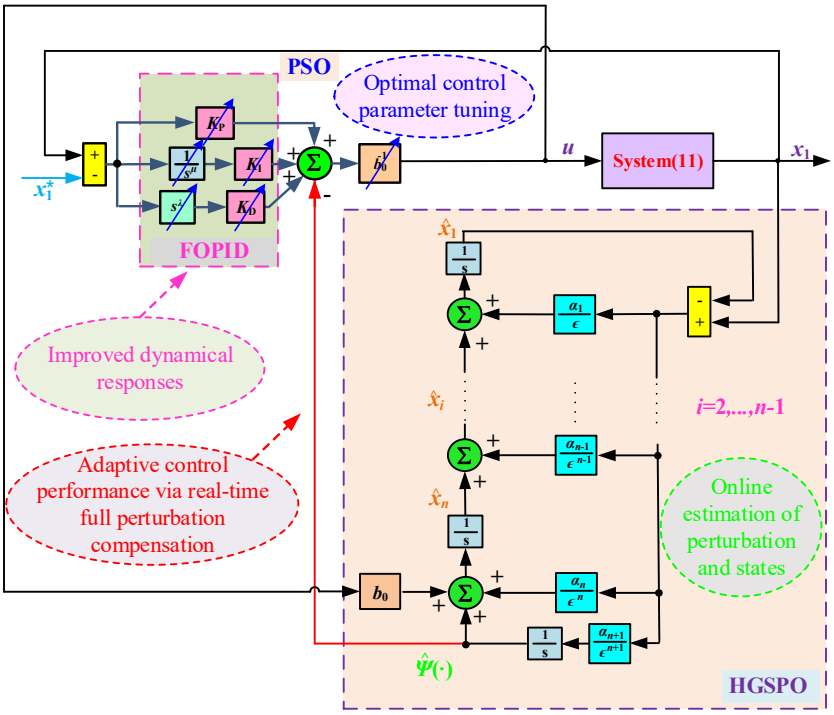


**Figure 2.** The overall control framework of AFOPID control.

The overall design procedure of AFOPID control for system (11) can be summarized as follows:

**Step 1:** Define perturbation (13) for the original *n*th-order system (11);

**Step 2:** Employ an extended state $x_{n+1} = \psi(\cdot)$ to represent perturbation (13);

**Step 3:** Extend the original *n*th-order system (11) into the extended (*n*+1)th-order system (15);

**Step 4:** Use the (*n*+1)th-order HGSPO (16) for the extended (*n*+1)th-order system (15) to simultaneously estimate the state estimate $\hat{x}$ and perturbation estimate $\hat{\psi}(\cdot)$ online with the only measurement of the output $y=x_1$;

**Step 5:** Design AFOPID control (20) for the original *n*th-order system (11).

## 4 AFOPID Control Design of PMSG for MPPT

Define the tracking error $e = [e_1,\ e_2]^{\mathrm{T}} = [i_{\mathrm{d}}\text{-}i_{\mathrm{d}}^*,\ \omega_{\mathrm{m}}\text{-}\omega_{\mathrm{m}}^*]^{\mathrm{T}}$, with $i_{\mathrm{d}}^*$ and $\omega_{\mathrm{m}}^*$ being the d-axis current reference and mechanical rotation speed reference, respectively. Differentiate the tracking error $e$ until the control input $u = [u_1,\ u_2]^{\mathrm{T}} = [V_{\mathrm{d}},\ V_{\mathrm{q}}]^{\mathrm{T}}$ appears explicitly, yield

$$\begin{bmatrix}\dot{e}_1\\ \ddot{e}_2\end{bmatrix} = \begin{bmatrix}f_1(\cdot)\\ f_2(\cdot)\end{bmatrix} + B\begin{bmatrix}u_1\\ u_2\end{bmatrix} - \begin{bmatrix}\dot{i}_{\mathrm{d}}^*\\ \ddot{\omega}_{\mathrm{m}}^*\end{bmatrix} \tag{21}$$

where

$$f_1(x) = -\frac{R_{\mathrm{s}}}{L_{\mathrm{d}}} i_{\mathrm{d}} + \frac{\omega_{\mathrm{e}} L_{\mathrm{q}}}{L_{\mathrm{d}}} i_{\mathrm{q}} \tag{22}$$

$$f_2(x) = \frac{\dot{T}_{\mathrm{m}}}{J_{\mathrm{tot}}} - \frac{p i_{\mathrm{q}}}{J_{\mathrm{tot}} L_{\mathrm{d}}}\left(L_{\mathrm{d}} - L_{\mathrm{q}}\right)\left(-R_{\mathrm{s}} i_{\mathrm{d}} + L_{\mathrm{q}} \omega_{\mathrm{e}} i_{\mathrm{q}}\right) + \frac{p}{J_{\mathrm{tot}} L_{\mathrm{q}}}\left[K_{\mathrm{e}} + \left(L_{\mathrm{d}} - L_{\mathrm{q}}\right) i_{\mathrm{d}}\right]\left(L_{\mathrm{d}} \omega_{\mathrm{e}} i_{\mathrm{d}} + R_{\mathrm{s}} i_{\mathrm{q}} + \omega_{\mathrm{e}} K_{\mathrm{e}}\right) \tag{23}$$

with

$$B(x) = \begin{bmatrix} \frac{1}{L_{\mathrm{d}}} & 0 \\ -\frac{p i_{\mathrm{q}}}{J_{\mathrm{tot}} L_{\mathrm{d}}}\left(L_{\mathrm{d}} - L_{\mathrm{q}}\right) & -\frac{p}{J_{\mathrm{tot}} L_{\mathrm{q}}}\left[K_{\mathrm{e}} + \left(L_{\mathrm{d}} - L_{\mathrm{q}}\right) i_{\mathrm{d}}\right] \end{bmatrix} \tag{24}$$

Here, functions $f_1(x)$, $f_2(x)$ and matrix $B(x)$ represent the combinatorial effect of the generator nonlinearities and parameter uncertainties, as well as stochastic wind speed variation. In practice, their accurate values are difficult to obtain thus need to be estimated by HGSPO.

In order to make the above input-output linearization valid, the control gain matrix $B(x)$ is required to be nonsingular in its whole operation range, thus

$$\det[B(x)] = -\frac{p[K_{\mathrm{e}} + (L_{\mathrm{d}} - L_{\mathrm{q}}) i_{\mathrm{d}}]}{J_{\mathrm{tot}} L_{\mathrm{d}} L_{\mathrm{q}}} \neq 0 \tag{25}$$

which can be always satisfied when $K_{\mathrm{e}} \neq -(L_{\mathrm{d}} - L_{\mathrm{q}}) i_{\mathrm{d}}$.

Define the perturbations $\psi_1(\cdot)$ and $\psi_2(\cdot)$ for tracking error dynamics (21) to aggregate all the PMSG nonlinearities and parameter uncertainties, as well as wind speed randomness into a lumped term, as follows

$$\begin{bmatrix}\psi_1(\cdot)\\ \psi_2(\cdot)\end{bmatrix}=\begin{bmatrix}f_1(x)\\ f_2(x)\end{bmatrix}+(B(x)-B_0)\begin{bmatrix}u_1\\ u_2\end{bmatrix} \tag{26}$$

and the constant control gain matrix $B_0$ is chosen in the diagonal form, such that the control of d-axis current and mechanical rotation speed can be fully decoupled, it gives

$$B_0=\begin{bmatrix}b_{11} & 0\\ 0 & b_{22}\end{bmatrix} \tag{27}$$

where $b_{11}$ and $b_{22}$ are constant control gains of PMSG.

Hence, tracking error dynamics (21) can be rewritten in terms of perturbation and constant control gain matrix by

$$\begin{bmatrix}\dot{e}_1\\ \ddot{e}_2\end{bmatrix}=\begin{bmatrix}\psi_1(\cdot)\\ \psi_2(\cdot)\end{bmatrix}+B_0\begin{bmatrix}u_1\\ u_2\end{bmatrix}-\begin{bmatrix}\dot{i}_{\mathrm{d}}^*\\ \ddot{\omega}_{\mathrm{m}}^*\end{bmatrix} \tag{28}$$

For the second-order d-axis current dynamics, there exist no internal state which needs to be estimated or measured, thus a second-order high-gain perturbation observer (HGPO) is employed to estimate perturbation $\psi_1(\cdot)$ as

$$\begin{cases}\dot{\hat{i}}_{\mathrm{d}}=\hat{\psi}_1(\cdot)+\frac{\alpha_{11}}{\epsilon_1}(i_{\mathrm{d}}-\hat{i}_{\mathrm{d}})+b_{11}u_1\\ \dot{\hat{\psi}}_1(\cdot)=\frac{\alpha_{12}}{\epsilon_1^2}(i_{\mathrm{d}}-\hat{i}_{\mathrm{d}})\end{cases} \tag{29}$$

where Luenberger observer gains $\alpha_{11}$ and $\alpha_{12}$ are all positive constants, with $0\le\epsilon_1\ll 1$.

Meanwhile, a third-order HGSPO is applied to estimate perturbation $\psi_2(\cdot)$ and one internal state, e.g., the first-order derivative of mechanical rotation speed, as follows

$$\begin{cases}\dot{\hat{\omega}}_{\mathrm{m}}=\hat{\omega}_m+\frac{\alpha_{21}}{\epsilon_2}(\omega_{\mathrm{m}}-\hat{\omega}_{\mathrm{m}})\\ \dot{\hat{\omega}}_{\mathrm{m}}=\hat{\psi}_2(\cdot)+\frac{\alpha_{22}}{\epsilon_2^2}(\omega_{\mathrm{m}}-\hat{\omega}_{\mathrm{m}})+b_{22}u_2\\ \dot{\hat{\psi}}_2(\cdot)=\frac{\alpha_{23}}{\epsilon_2^3}(\omega_{\mathrm{m}}-\hat{\omega}_{\mathrm{m}})\end{cases} \tag{30}$$

where observer gains $\alpha_{21}$, $\alpha_{22}$, and $\alpha_{23}$ are all positive constants, with $0\le\epsilon_2\ll 1$.

The AFOPID control for tracking error dynamics (28) can be designed by

$$\begin{bmatrix}u_1\\ u_2\end{bmatrix}=B_0^{-1}\begin{bmatrix}\dot{i}_{\mathrm{d}}^*-\hat{\psi}_1(\cdot)+K_{\mathrm{P1}}(i_{\mathrm{d}}-i_{\mathrm{d}}^*)+\frac{K_{\mathrm{I1}}}{s^{\mu_1}}(i_{\mathrm{d}}-i_{\mathrm{d}}^*)+K_{\mathrm{D1}}s^{\lambda_1}(i_{\mathrm{d}}-i_{\mathrm{d}}^*)\\ \ddot{\omega}_{\mathrm{m}}^*-\hat{\psi}_2(\cdot)+K_{\mathrm{P2}}(\omega_{\mathrm{m}}-\omega_{\mathrm{m}}^*)+\frac{K_{\mathrm{I2}}}{s^{\mu_2}}(\omega_{\mathrm{m}}-\omega_{\mathrm{m}}^*)+K_{\mathrm{D2}}s^{\lambda_2}(\omega_{\mathrm{m}}-\omega_{\mathrm{m}}^*)\end{bmatrix} \tag{31}$$

where PID control gains $K_{\mathrm{P1}}$, $K_{\mathrm{P2}}$, $K_{\mathrm{I1}}$, $K_{\mathrm{I2}}$, $K_{\mathrm{D1}}$, $K_{\mathrm{D2}}$, fractional integrator order $\mu_1$ and $\mu_2$, differentiator order $\lambda_1$ and $\lambda_2$, are chosen to realize a satisfactory convergence of tracking error dynamics (20).

The AFOPID control parameters in Eq. (31) and observer gains in Eq. (29) and Eq. (30) are optimally tuned through PSO [35] under three cases, e.g., (a) step change of wind speed; (b) low-turbulence stochastic wind speed; and (c) high-turbulence stochastic wind speed. The optimization goal is to minimize the tracking error of mechanical rotation speed and d-axis current, together with the corresponding control costs, which model is given as follows

$$\text{Minimize } F(\mathrm{x})=\sum_{\text{Three cases}}\int_0^T(|\omega_{\mathrm{m}}-\omega_{\mathrm{m}}^*|+|i_{\mathrm{d}}-i_{\mathrm{d}}^*|+\omega_1|u_1|+\omega_2|u_2|)\,\mathrm{d}t$$

$$\text{subject to }\begin{cases}K_{\mathrm{P}i}^{\min}\le K_{\mathrm{P}i}\le K_{\mathrm{P}i}^{\max}\\ K_{\mathrm{I}i}^{\min}\le K_{\mathrm{I}i}\le K_{\mathrm{I}i}^{\max}\\ K_{\mathrm{D}i}^{\min}\le K_{\mathrm{D}i}\le K_{\mathrm{D}i}^{\max}\\ \lambda_i^{\min}\le\lambda_i\le\lambda_i^{\max}\\ \mu_i^{\min}\le\mu_i\le\mu_i^{\max}\\ \lambda_{\alpha i}^{\min}\le\lambda_{\alpha i}\le\lambda_{\alpha i}^{\max}\\ b_{ii}^{\min}\le b_{ii}\le b_{ii}^{\max}\\ u_i^{\min}\le u_i\le u_i^{\max}\end{cases},\qquad i=1,2. \tag{32}$$

where the weights $\omega_1$ and $\omega_2$ are used to scale the magnitude of control costs which are chosen to be 1/5. $T$=25 s denotes the simulation time.

The proportional gains $K_{\mathrm{P}i}$ lie in [-400, 0], integral gains $K_{\mathrm{I}i}$ is between [-600, 0], derivative gains $K_{\mathrm{D}i}$ is among [-100, 0], fractional integrator orders $\mu_i$ and differentiator orders $\lambda_i$ are bounded in [0, 2], observer roots $\lambda_{\alpha i}$ is located in [10, 50], constant control gains $b_{ii}$ is chosen among [-8000, 0], respectively. Besides, the thickness layer boundary of observer $\epsilon_1$=$\epsilon_2$ =0.1. As the control inputs may exceed the admissible capacity of the generator side VSC at some operation points, their values are bounded in [-0.65, 0.65] per unit (p.u.). The PSO parameters are chosen as the total number of iteration $N$=80, minimum velocity $v_{\min}$=0.1, maximum velocity $v_{\max}$=1, weight coefficients $c_1/c_2$=2/2, iteration index $k$=2, respectively [35]. In addition, the convergence criteria is chosen as

$$|F_j-F_{j-1}|\le\varepsilon \tag{33}$$

where $\varepsilon$ is the tolerance of convergence error, which value is chosen to be $10^{-4}$ in this paper; $F_j$ and $F_{j-1}$ represent the fitness function value calculated at the $j$th iteration and the ($j$-1)th iteration, respectively.

To this end, Figure 3 describes the overall AFOPID control structure of PMSG for MPPT. Here, only the d-axis current $i_{\mathrm{d}}$ and mechanical rotation speed $\omega_{\mathrm{m}}$ need to be measured. Lastly, the obtained control inputs are modulated by the sinusoidal pulse-width modulation (SPWM) technique [29,30].

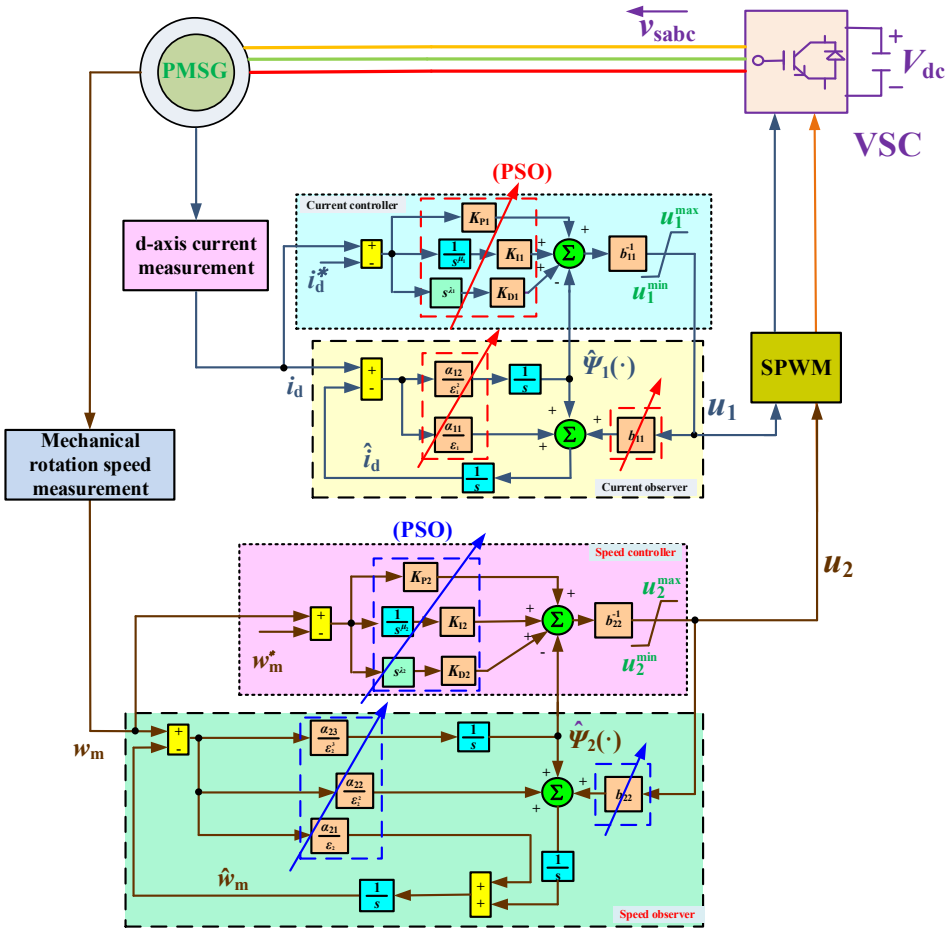


**Figure 3.** The overall AFOPID control structure of PMSG for MPPT.

## 5 Case Studies

The proposed AFOPID control is applied on PMSG for MPPT while the PMSG based WECS parameters are tabulated in Table 1. The control performance of AFOPID control is evaluated and compared to that of conventional PID control [12], FOPID control [16], and FLC [17], respectively. Here, In order to achieve a fair comparison, the parameters of these four controllers are all optimally tuned by PSO. In particularly, the control parameter range of PIF control and FOPID control is the same to that of AFOPID control given in previous section, while the control parameter range of FLC is bounded as $\lambda_1 \in[0, 40]$ and $\lambda_2 \in[0, 50]$. Moreover, PSO runs for 30 times and the best results are adopted for each controller. The obtained optimal control parameters of each controller can be found in Table 2 while the statistic results are tabulated in Table 3, respectively. From Table 3, it can be seen that FLC just needs the shortest convergence time as it has only two control parameters that need to be tuned. Moreover, FOPID control can obtain a lower fitness function than that of PID control due to the fractional-order mechanism. At last, AFOPID control owns the lowest fitness function thus it has the best performance among all controllers.

**Table 1.** The PMSG based WECS parameters

| | | | | | |
|---|---|---|---|---|---|
| **PMSG rated power** | $P_{\mathrm{base}}$ | 2 MW | **Field flux** | $K_{\mathrm{e}}$ | 136.25 V·s/rad |
| **Radius of wind turbine** | $R$ | 39 m | **Pole pairs** | $p$ | 11 |

| | | | | | |
|---|---|---|---|---|---|
| **d-axis stator inductance** | $L_{\mathrm{d}}$ | 5.5 mH | **Air density** | $\rho$ | 1.205 kg/m$^3$ |
| **q-axis stator inductance** | $L_{\mathrm{q}}$ | 3.75 mH | **Rated wind speed** | $v_{\mathrm{wind}}$ | 12 m/s |
| **Total inertia** | $J_{\mathrm{tot}}$ | 10000 kg·m$^2$ | **Stator resistance** | $R_{\mathrm{s}}$ | 50 $\mu\Omega$ |

**Table 2.** The optimal control parameters of different controllers obtained by PSO in 30 runs.

| | **d-axis current** | | | **mechanical rotation speed** | | |
|---|---|---|---|---|---|---|
| **PID** | $K_{\mathrm{P1}} = -243$ | $K_{\mathrm{I1}} = -458$ | $K_{\mathrm{D1}} = -16$ | $K_{\mathrm{P2}} = -305$ | $K_{\mathrm{I2}} = -474$ | $K_{\mathrm{D2}} = -23$ |
| **FOPID** | $K_{\mathrm{P1}} = -177$ | $K_{\mathrm{I1}} = -344$ | $K_{\mathrm{D1}} = -10$ | $K_{\mathrm{P2}} = -379$ | $K_{\mathrm{I2}} = -582$ | $K_{\mathrm{D2}} = -67$ |
| | $\mu_1 = 1.18$ | $\lambda_1 = 1.65$ | | $\mu_2 = 1.72$ | $\lambda_2 = 0.85$ | |
| **FLC** | $\lambda_1 = 25$ | | | $\lambda_2 = 40$ | | |
| **AFOPID** | $K_{\mathrm{P1}}$=-120 | $K_{\mathrm{I1}}$=-250 | $K_{\mathrm{D1}}$=-45 | $K_{\mathrm{P2}}$=-80 | $K_{\mathrm{I2}}$=-180 | $K_{\mathrm{D2}}$=-15 |
| | $\mu_1 = 1.5$ | $\lambda_1 = 0.75$ | $b_{11} = -2000$ | $\mu_2 = 1.25$ | $\lambda_2 = 0.5$ | $b_{22}$=−4500 |
| | $\alpha_{11}$= 40 | $\alpha_{12}$= 400 | | $\alpha_{21}$=30 | $\alpha_{22}$=300 | $\alpha_{23}$=1000 |

**Table 3.** The statistical results of obtained by different controllers in 30 runs.

| **Algorithm** | **Fitness function (p.u.)** | | | **Convergence time (hour)** | | | **Iteration number of convergence** | | |
|---|---|---|---|---|---|---|---|---|---|
| | **Max.** | **Min.** | **Mean** | **Max.** | **Min.** | **Mean** | **Max.** | **Min.** | **Mean** |
| **PID** | 2.08 | 1.57 | 1.74 | 0.22 | 0.12 | 0.16 | 121 | 89 | 105 |
| **FOPID** | 1.64 | 1.33 | 1.42 | 0.26 | 0.17 | 0.21 | 132 | 98 | 113 |
| **FLC** | 1.28 | 1.02 | 1.15 | 0.09 | 0.04 | 0.07 | 36 | 15 | 24 |
| **AFOPID** | 1.09 | 0.86 | 0.97 | 0.45 | 0.32 | 0.38 | 145 | 127 | 136 |

### *5.1. Step change of wind speed*

At first, four consecutive step changes of wind speed increased from 8 m/s to 12 m/s with 10 m/s$^2$ rate are tested, which attempt to simulate a series of sudden gust. Meanwhile, the d-axis current reference varies to study the control performance of AFOPID control. The wind speed profile and the corresponding PMSG responses are shown in Fig. 4, which demonstrates that PID control presents the highest active power overshoot during each step change of wind speed, as well as the slowest tracking rate. In addition, FOPID control can reduce the overshoot with a faster tracking rate thanks to the two additional adjustable coefficients, thus the transient responses can be considerably improved. However, they both have an inconsistent control performance when operation points vary due to the one-point linearization.

In contrast, FLC and AFOPID control can offer a global control consistency since the all the PMSG nonlinearities are fully compensated. However, AFOPID control only need the measurement of d-axis current and mechanical rotation speed while FLC requires the full state measurement and PMSG parameters. Hence, AFOPID control structure is much simpler than that of FLC.

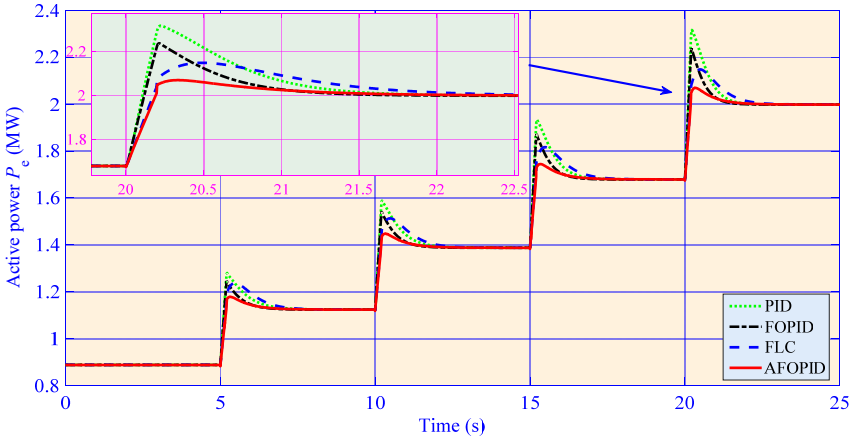


**(a)** Step change of wind speed

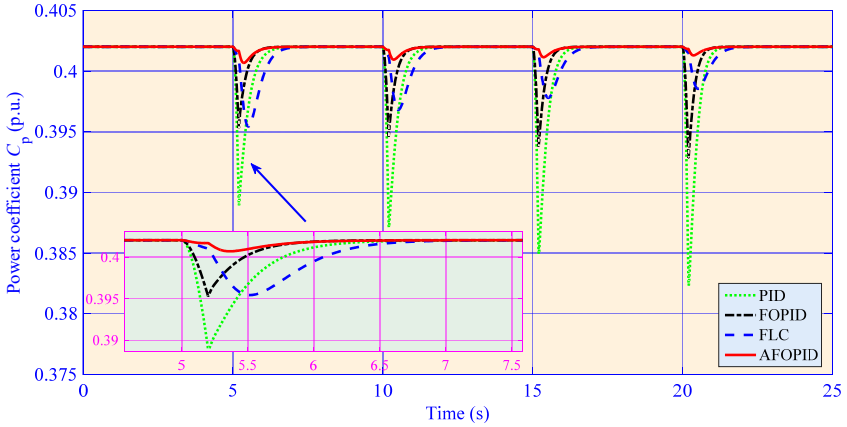


**(b)** Power coefficient

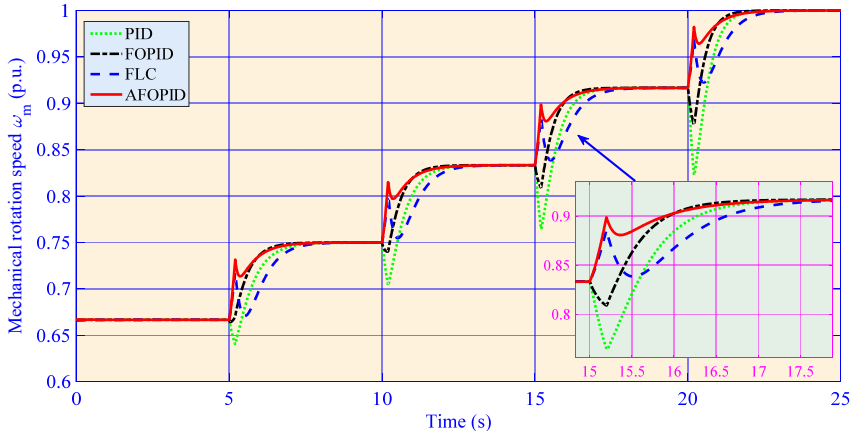


**(c)** Mechanical rotational speed

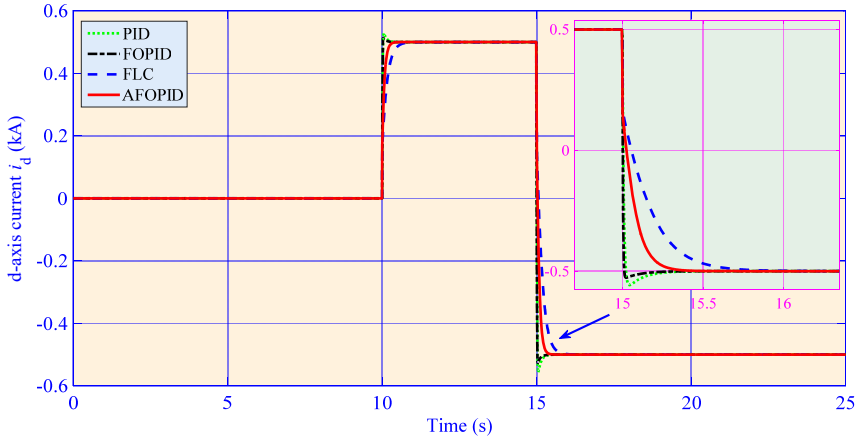


**(d)** d-axis current

**Figure 4.** PMSG responses obtained under four consecutive step changes of wind speed started from 8 m/s and ended at 12 m/s. (a): Step change of wind speed; (b): Power coefficient; (c): Mechanical rotational speed; (d): d-axis current

### *5.2. Low-turbulence stochastic wind speed*

A low-turbulence stochastic wind speed varies between 7 m/s to 11 m/s are investigated to, which aims to mimic a general wind variation [31]. The corresponding PMSG responses are demonstrated by Fig. 5, from which it can observe that the power coefficient of AFOPID control is the closest to the optimum among all controllers, such that it can extract the maximum power from wind. This is because that the stochastic wind speed variation can be rapidly estimated by HGSPO and fully compensated by the controller in the real-time.

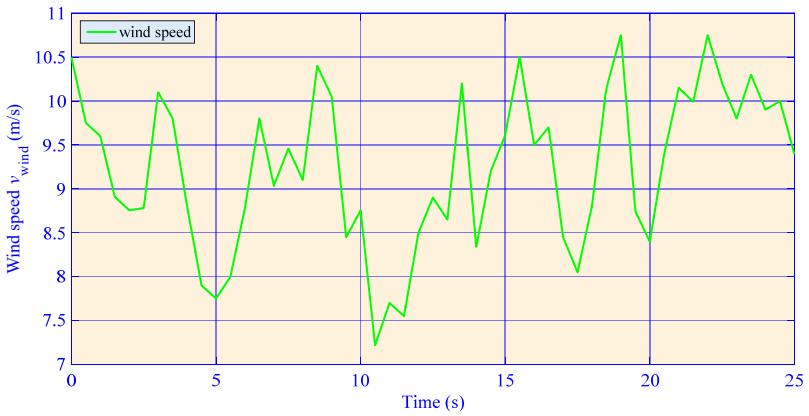


(a) Wind speed profile

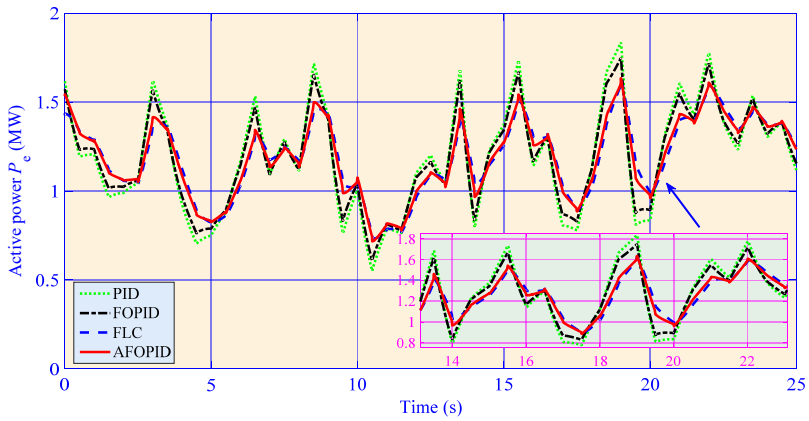


(b) Active power

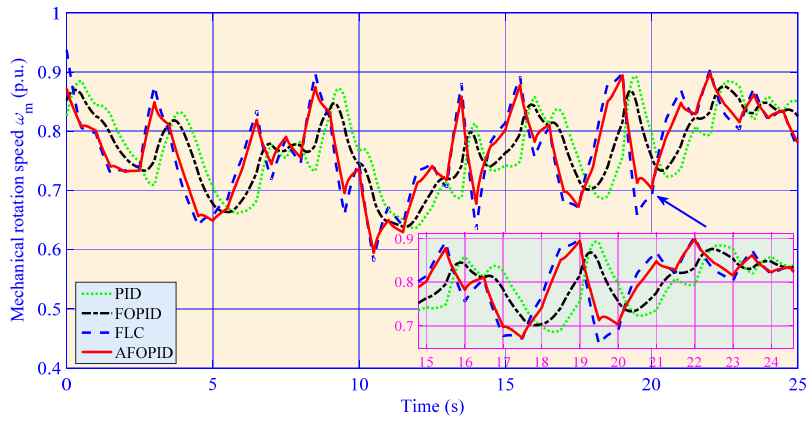


(c) Mechanical rotational speed

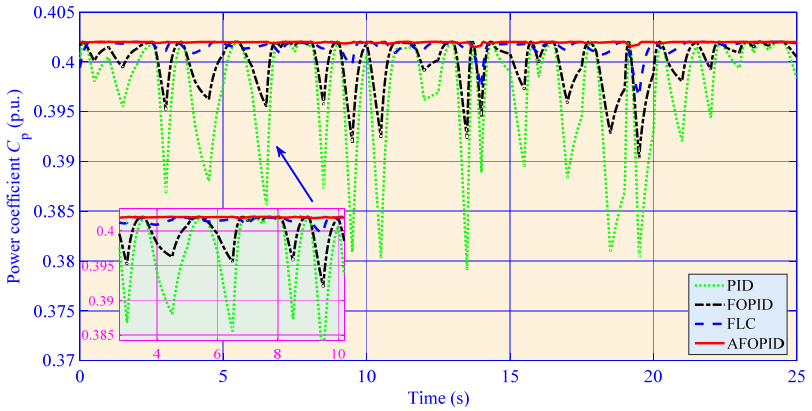


(d) Power coefficient

**Figure 5** PMSG responses obtained under a low-turbulence stochastic wind speed between 7 m/s to 11 m/s. (a): Wind speed profile; (b):Active power; (c): Mechanical rotational speed; (d): Power coefficient

### *5.3. High-turbulence stochastic wind speed*

In some extreme weather conditions, i.e., plateau, coast, desert etc., the wind speed might dramatically change which makes the MPPT a very challenging task as it requires a rapid and timely controller response. Here, a high-turbulence stochastic wind speed varying among 6 m/s to 12 m/s is tested to study the MPPT performance of each approaches. The PMSG responses are illustrated in Fig. 6, in which one can find that AFOPID control can still maintain a satisfactory control performance and outperform other methods associated with maximum power extraction, lowest power overshoot, and fastest tracking rate.

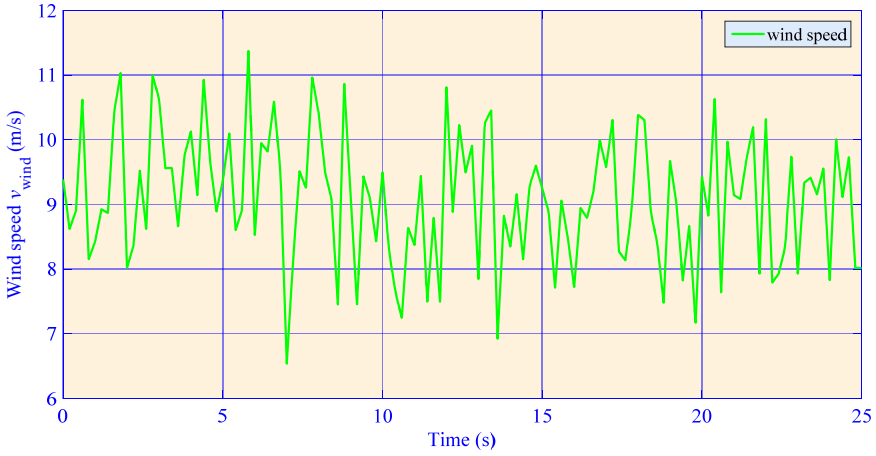


(a) Wind speed profile

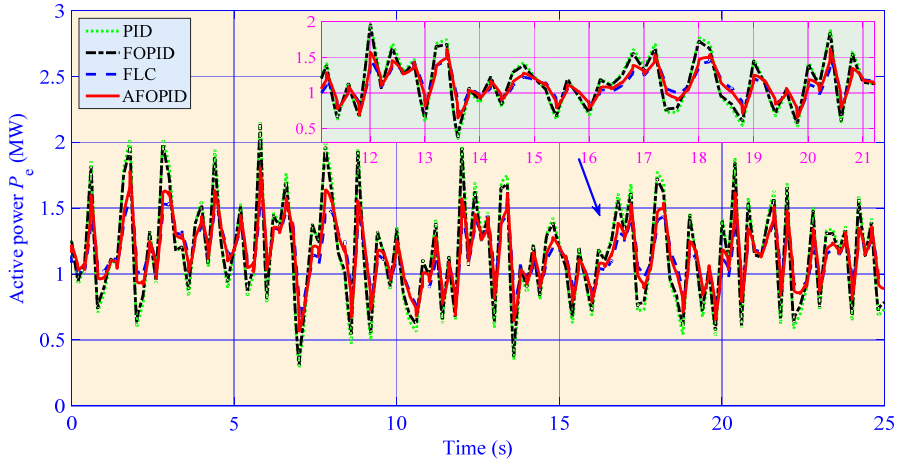


(b) Active power

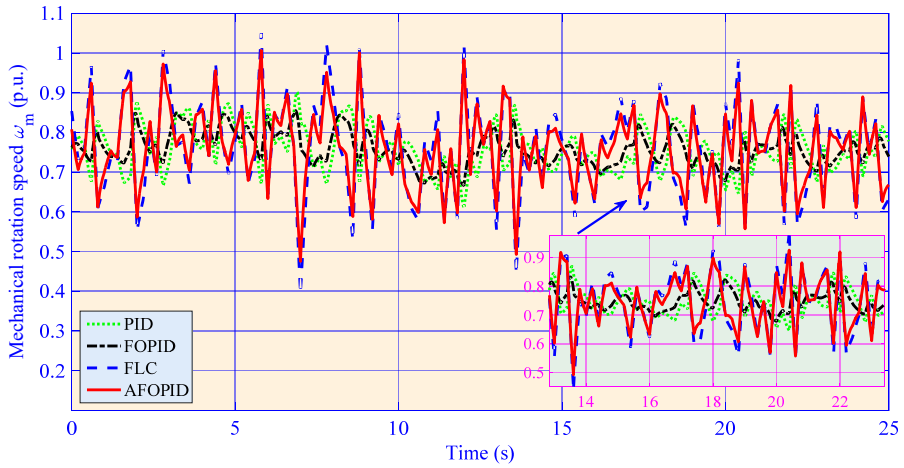


(c) Mechanical rotational speed

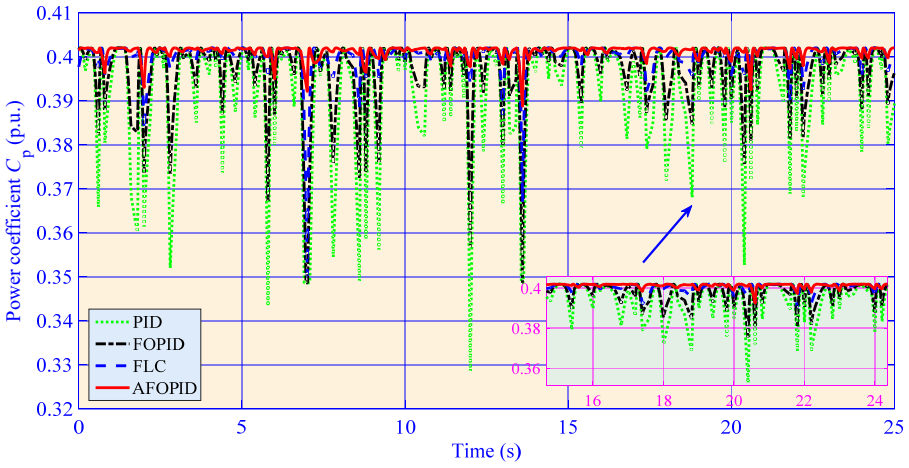


(d) Power coefficient

**Figure 6.** System responses obtained under a high-turbulence stochastic wind speed between 6 m/s to 12 m/s. (a): Wind speed profile; (b):Active power; (c): Mechanical rotational speed; (d): Power coefficient

### *5.4. Generator parameter uncertainties*

It is worth noting that the accurate generator parameters are usualy difficult to obtain as their values might be affected by the ambient environment temperature, wear-and-tear, generator aging, pressure, measurement error, ect. [32-34], such that the use of their nominal value in the controller loop would somehow resul in an inaccurate response, particularly when a PMSG has operated for years. Hence, it is quite crucial to study the robustness of the proposed controller. Here, a series of plant-model mismatches of stator resistance $R_s$ and d-axis inductance $L_d$ associated with ±20% variation around their nominal

value are carried out, in which a 1 m/s step increase of wind speed from the rated value (12 m/s) is applied and the peak absolute value of active power $|P_e|$ of each controller is compared. Figure 7 shows that the variation of $|P_e|$ obtained by PID control, FOPID control, FLC, and AFOPID control is 16.1%, 13.7%, 23.4%, 9.5%, respectively. As a consequence, AFOPID control is able to effectively avoid the control performance degradation resulted from generator parameter uncertainties via real-time perturbation compensation, thus it can offer the strongest robustness.

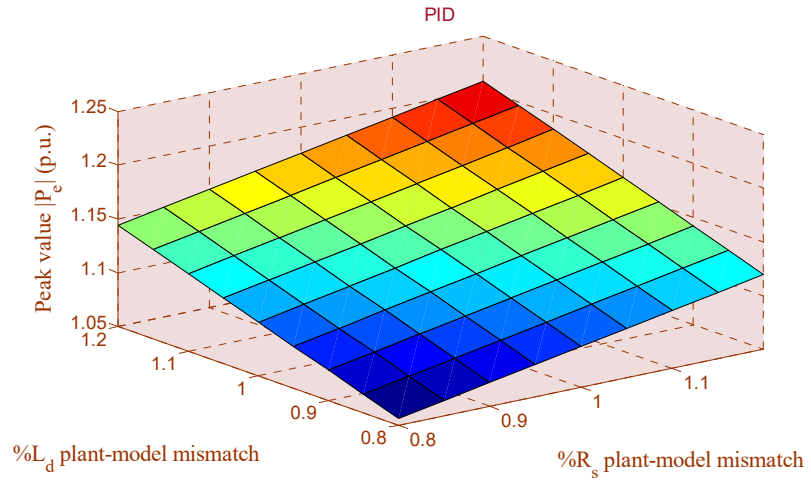


(a) PID control

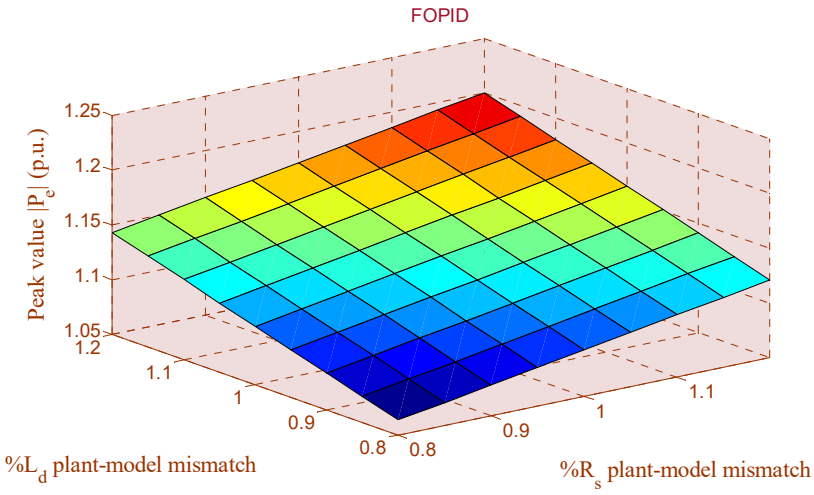


(b) FOPID control

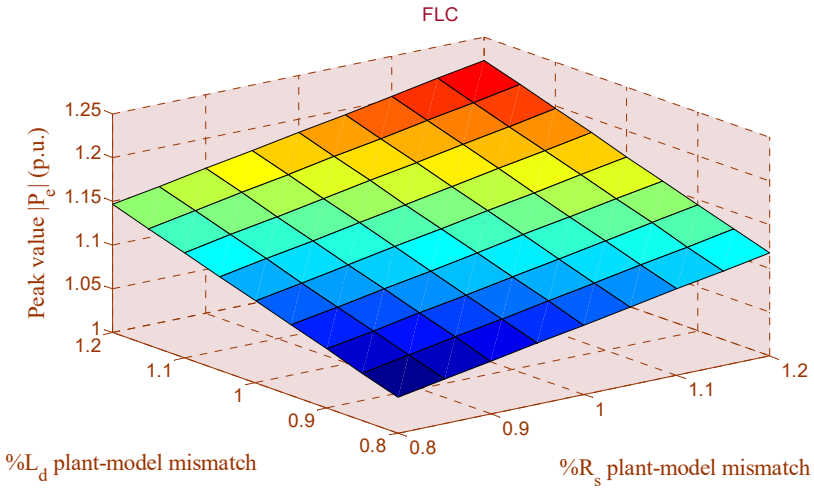

(c) FLC

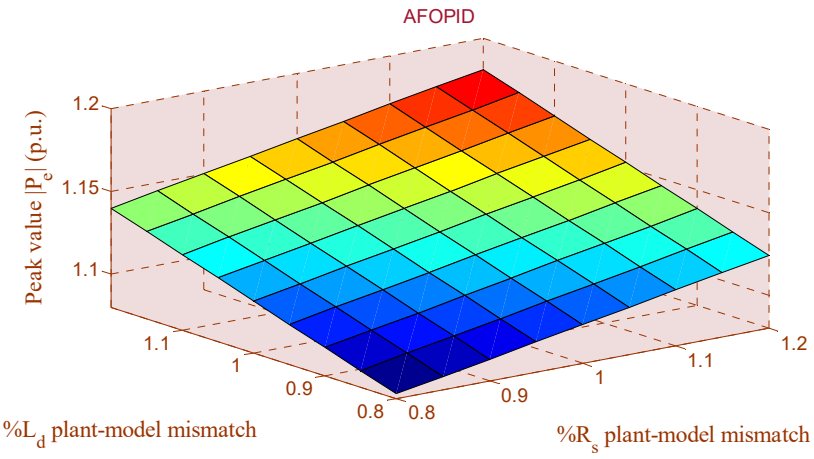


(d) AFOPID control

**Figure 7.** Peak value of active power $|P_e|$ obtained under a 1 m/s step increase of wind speed from the rated value (12 m/s) with 20% variation of the stator resistance $R_s$ and d-axis inductance $L_d$ of three approaches, respectively. (a): PID; (b):FOPID (c): FLC; (d): AFOPID

### *5.5. Comparative studies*

In order to quantatively compare the control performance of each controller, the integral of absolute error (IAE) indices are employed, where $\text{IAE}_x = \int_0^T |x - x^*| \, \mathrm{d}t$ with the simulation time $T$ =25 s. Table 4 shows that AFOPID control owns the lowest IAE indices of mechanical rotation speed and d-axis current (in bold) in all cases. In particular, its IAE$\omega_m$ obtained in high-turbulence stochastic wind speed is merely 63.72%, 67.85%, and 71.72% to that of PID control, FOPID control, and FLC, respectively. As a result, it can achieve the most satisfactory MPPT performance with moderate structure complexity.

**Table 4.** IAE indices of four controllers obtained in three cases (p.u.)

| Case | Step change of wind speed | Low-turbulence stochastic wind speed | High-turbulence stochastic wind speed |
|---|---|---|---|
| Controller | **IAE index IAE$\omega_m$ of mechanical rotation speed** | | |
| PID | 1.46E-01 | 6.77E-01 | 9.87E-01 |
| FOPID | 1.21E-01 | 6.35E-01 | 9.27E-01 |
| FLC | 1.02E-01 | 5.86E-01 | 8.77E-01 |
| AFOPID | **8.16E-02** | **4.97E-01** | **6.29E-01** |
| Controller | **IAE index IAE$_{id}$ of d-axis current** | | |
| PID | 1.58E-02 | 6.48E-03 | 8.21E-03 |
| FOPID | 1.26E-02 | 6.09E-03 | 7.79E-03 |
| FLC | 9.68E-03 | 5.54E-03 | 7.15E-03 |
| AFOPID | **8.87E-03** | **4.23E-03** | **6.17E-03** |

Finally, the overall control costs of each controllers required in three cases are illustrated by Fig. 8, which is calculated as $\int_0^T (|u_1 - u_1^*| + |u_2 - u_2^*|)\mathrm{d}t$. One can find that AFOPID control just requires the minimum overall control costs in all cases among all controllers thanks to the real-time perturbation compensation. Particularly, the summed control costs of AFOPID control of three cases is just 87.60%, 90.82%, and 93.63% to that of PID control, FOPID control, and FLC, respectively.

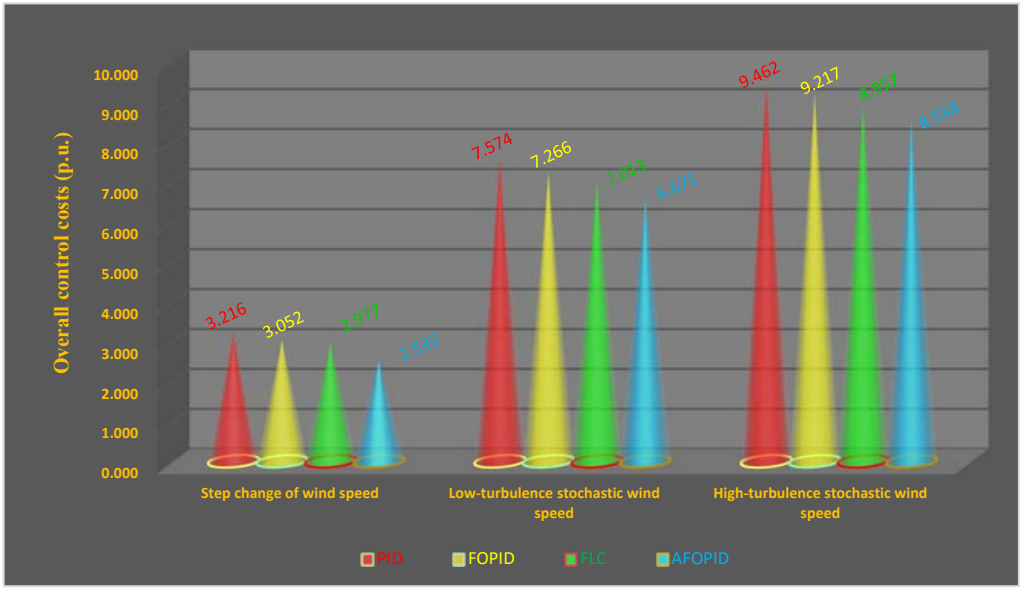


**Figure 8.** Overall control costs required by four controllers under three cases.

## 6. Conclusions

In this paper, a novel AFOPID control is proposed for PMSG based WECS to extract the maximum power from various wind speed, while the main contributions can be summarized into the following four aspects:

(1) An HGSPO is used to simultaneously estimate the PMSG nonlinearities and parameter uncertainties, unmodelled dynamics, as well as stochastic wind speed variation in the real-time, which is then fully compensated by an FOPID controller. Thus, AFOPID control can effectively handle complex nonlinearities and various modelling uncertainties;

(2) The merits of globally robust control consistency of nonlinear robust/adaptive control and advantages of structure simplicity of FOPID framework are beneficially incorporated by AFOPID control, while its control structure complexity is moderate;

(3) AFOPID control does not require an accurate PMSG system model while only the d-axis current and mechanical rotation speed need to be measured. Moreover, a fully decoupled control of mechanical rotation speed and d-axis current is achieved as the constant control gain matrix is chosen in the diagonal form. Hence, AFOPID control is quite easy to be implemented in practice;

(4) Simulation results verify that AFOPID control can realize a globally robust control consistency while optimally extract the wind power from various wind speed, together with a relatively low control costs among all approaches.

Future studies will be focused on the following two directions:

(a) Apply AFOPID control on the grid-side VSC to enhance the low-voltage ride-through (LVRT) capability of PMSG;

(b) Validate the implementation feasibility of AFOPID control via the real-time digital simulator (RTDS) based hardware-in-loop (HIL) test.

**Acknowledgments:** The authors gratefully acknowledge the support of National Natural Science Foundation of China (51477055, 51667010, 51777078). Yunnan Provincial Talents Training Program (KKSY201604044), and Scientific Research Foundation of Yunnan Provincial Department of Education (2017ZZX146).

## References

[1] Wang, J.; Wang, X.; Zeng, P.; Sun, P. Design of a weekly hybrid power market in China facilitating connection of large-scale renewable generation. *International Transactions on Electrical Energy Systems* **2015**, 25(9):1697-1716.

[2] Liao, S. W.; Yao, W.; Han, X. N.; Wen, J. Y.; Cheng, S. J. Chronological operation simulation framework for regional power system under high penetration of renewable energy using meteorological data. *Applied Energy* **2017**, 203, 816-828.

[3] Shen, Y.; Yao, W.; Wen, J. Y.; He, H. B. Adaptive wide-area power oscillation damper design for photovoltaic plant considering delay compensation. *IET Generation, Transmission and Distribution* **2017**, 11(18): 4511-4519.

[4] Liu, J.; Wen, J. Y.; Yao, W.; Long, Y. Solution to short-term frequency response of wind farms by using energy storage systems. *IET Renewable Power Generation* **2016**, 10(5): 669-678.

[5] Shen, Y.; Yao, W.; Wen, J. Y.; He, H. B.; Chen, W. B. Adaptive supplementary damping control of VSC-HVDC for interarea oscillation using GrHDP. *IEEE Transactions on Power Systems* **2018**, 33(2): 1777-1789.
[6] Hu, F.; Hughes, K.J.; Ma, L.; Pourkashanian, M. Combined economic and emission dispatch considering conventional and wind power generating units. *International Transactions on Electrical Energy Systems*, **2017**, 27, e2424.
[7] Yang, B.; Zhang, X.S.; Yu, T.; Shu, H.C.; Fang, Z.H. Grouped grey wolf optimizer for maximum power point tracking of doubly-fed induction generator based wind turbine. *Energy Conversion and Management* **2017**, 133, 427-443.
[8] Yang, B.; Jiang, L.; Wang, L.; Yao, W.; Wu, Q.H. Nonlinear maximum power point tracking control and modal analysis of DFIG based wind turbine. *International Journal of Electrical Power and Energy Systems* **2016**, 74, 429-436.
[9] Tripathi, S.M.; Tiwari, A.N.; Singh, D. Optimum design of proportional−integral controllers in grid−integrated PMSG−based wind energy conversion system. *International Transactions on Electrical Energy Systems* **2016**, 26(5):1006-1031.
[10] Bonfiglio, A.; Delfino, F.; Gonzalez-Longatt, F.; Procopio, R. Steady-state assessments of PMSGs in wind generating units. *International Journal of Electrical Power and Energy Systems* **2017**, 90, 87-93.
[11] Song, D.R.; Yang, J.; Cai, Z.L.; Dong, M.; Su, M.; Wang, Y.H. Wind estimation with a non-standard extended Kalman filter and its application on maximum power extraction for variable speed wind turbines. *Applied Energy* **2017**, 190, 670-685.
[12] Li, S.H.; Haskew, T.A.; Xu, L. Conventional and novel control designs for direct driven PMSG wind turbines. *Electric Power Systems Research* **2010,** 80(3), 328-338.
[13] Ramadan, H.S. Optimal fractional order PI control applicability for enhanced dynamic behavior of on-grid solar PV systems. *International Journal of Hydrogen Energy* **2017**, 42, 4017-4031.
[14] Melicio, R.; Mendes, V.M.F.; Catalao, J.P.S. Fractional-order control and simulation of wind energy systems with PMSG/full-power converter topology. *Energy Conversion and Management* **2010**, 51, 1250-1258.
[15] Beddar, A.; Bouzekri, H.; Babes, B.; Afghoul, H. Experimental enhancement of fuzzy fractional order PI+I controller of grid connected variable speed wind energy conversion system. *Energy Conversion and Management* **2016**, 123, 569-580.
[16] Zheng, W.J.; Luo, Y.; Wang, X.H.; Pi, Y.G.; Chen, Y.Q. Fractional order $PI^{\lambda}D^{\mu}$ controller design for satisfying time and frequency domain specifications. *ISA Transactions* **2017**, 68, 212-222.
[17] Chen, J.; Jiang, L.; Yao, W.; Wu, Q.H. A feedback linearization control strategy for maximum power point tracking of a PMSG based wind turbine. *International Conference on Renewable Energy Research and Applications*, Madrid, Spain, 20-23 October **2013**, 79-84.
[18] Errami, Y.; Obbadi, A.; Sahnoun, S.; Benhmida, M.; Ouassaid, M.; Maaroufi, M. Design of a nonlinear backstepping control strategy of grid interconnected wind power system based PMSG. *Journal of Renewable & Sustainable Energy* **2016**, 1758(1):030053.
[19] Ikram, M.H.; Mohamed, W.N.; Najiba, M.B. Predictive control strategies for wind turbine system based on permanent magnet synchronous generator. *ISA Transactions* **2016**, 62, 73-80.
[20] Fantino, R.; Solsona, J.; Busada, C. Nonlinear observer-based control for PMSG wind turbine. *Energy* **2016**, 113, 248-257.
[21] Seyed, M.M.; Maarouf, S.; Hani, V.; Handy, F.B.; Mohsen, S. Sliding mode control of PMSG wind turbine based on enhanced exponential reaching law. *IEEE Transactions on Industrial Electronics* **2016** 63(10), 6148-6159.
[22] Yan, J.; Lin, H.; Feng, Y.; Guo, X.; Huang, Y.; Zhu, Z.Q. Improved sliding mode model reference adaptive system speed observer for fuzzy control of direct-drive permanent magnet synchronous generator wind power generation system. *IET Renewable Power Generation* **2013**, 7(1):28-35.
[23] Yang, B.; Jiang, L.; Yao, W.; Wu, Q.H. Perturbation estimation based coordinated adaptive passive control for multimachine power systems. *Control Engineering Practice* **2015**, 44:172-192.
[24] Yang, B.; Jiang, L.; Zhang, C.K.; Sang, Y.Y.; Yu, T.; Wu, Q.H. Perturbation observer based adaptive passive control for nonlinear systems with uncertainties and disturbances. *Transactions of the Institute of Measurement and Control* **2018**. 40(4): 1223-1236.
[25] Yang, B.; Yu, T.; Shu, H.C.; Zhang, Y.M.; Chen, J.; Sang, Y.Y.; Jiang, L. Passivity-based sliding-mode control design for optimal power extraction of a PMSG based variable speed wind turbine. *Renewable Energy* **2018**, 119: 577-589.
[26] Wu, Q.; Jiang, L.; Wen, J. Decentralized adaptive control of interconnected non-linear systems using high gain observer, *International Journal of Control* **2004**, 77(8): 703-712.
[27] Ramadan, H.S. Optimal fractional order PI control applicability for enhanced dynamic behavior of on-grid solar PV systems. *International Journal of Hydrogen Energy* **2017**, 42(7):4017-4031.
[28] Podlubny, I. Fractional differential equations, Academic Press, New York, 1999.
[29] Li, S.; Li, J. Output predictor-based active disturbance rejection control for a wind energy conversion system with PMSG. *IEEE Access* **2017**, 5:5205-5214.
[30] Zhao, Z.L.; Guo, B.Z. Nonlinear extended state observer based on fractional power functions. *Automatica* **2017**, 81:286-296.
[31] Verdejo, H.; Awerkin, A.; Saavedra, E.; Kliemann, W.; Vargas, L. Stochastic modeling to represent wind power generation and demand in electric power system based on real data. *Applied Energy* **2016**, 173:283-295.
[32] W. Yao, L. Jiang, J. Y. Wen, Q. H. Wu, S. J. Cheng. Wide-area damping controller for power system inter-area oscillations: a networked predictive control approach. *IEEE Transactions on Control Systems Technology*, **2015**, 23(1): 27-36.
[33] Yang, B.; Yu, T.; Shu, H.C.; Dong, J.; Jiang, L. Robust sliding-mode control of wind energy conversion systems for optimal power extraction via nonlinear perturbation observers. *Applied Energy* **2018**, 210: 711-723.
[34] Yang, B.; Yu, T.; Shu, H.C.; Zhang, X.S.; Qu, K.P.; Jiang, L. Democratic joint operations algorithm for optimal power extraction of PMSG based wind energy conversion system. *Energy Conversion and Management* **2018**, 159: 312-326.

[35] Kim, Y.S.; Chung, I.Y.; Moon, S.I. Tuning of the PI controller parameters of a PMSG wind turbine to improve control performance under various wind speeds. *Energies* **2015**; 8(2):1406–1425.